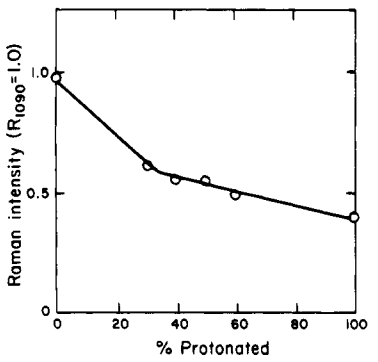

Figure 10. Plot of the relative intensity of the 1015–1020-cm^{-1} Raman band of 2% solutions of PVI in 0.88 M aqueous NaCl vs. extent of protonation.

and 915 cm^{-1} shift to 1511, 1096, and 945 cm^{-1}, respectively, upon metal incorporation.

B. The proton-bridged complex causing viscosity minima and double breaks in the potentiometric titration curves for PVI was characterized by FTIR and Raman spectra.

1. FTIR of dried films shows marker bands in the regions 2400–2600 and 900–950 cm^{-1} which appear to be associated with H bonding upon partial protonation. The band shifts in the 900–950-cm^{-1} region for protonated and Ni-complexed PVI suggest similar intrachain bridging or cross-linking in the two systems.

2. A conformational change of the backbone upon protonation is supported by the Raman spectra and is attributed to the formation of the H-bridged complexes.

Acknowledgment. We are grateful to Professor J. Koenig for discussion of some of the spectral assignments and to C. S. Baker and W. Brattlie for technical assistance.

Registry No. PVI (homopolymer), 25232-42-2.

References and Notes

(1) Tan, J. S.; Sochor, A. R. *Macromolecules* **1981**, *14*, 1700.
(2) Henrichs, P. M.; Whitlock, L. R.; Sochor, A. R.; Tan, J. S. *Macromolecules* **1980**, *13*, 1375.
(3) Handel, T. M.; Marshall, A. S.; Tan, J. S., to be submitted for publication.
(4) Cordes, M.; Walter, J. L. *Spectrochim. Acta, Part A* **1968**, *24a*, 237.
(5) Perchard, C.; Bellocq, A. M.; Novak, A. *J. Chim. Phys. Phys.-Chim. Biol.* **1965**, *62*, 1344.
(6) Perchard, C.; Novak, A. *Spectrochim. Acta, Part A* **1967**, *23a*, 1953.
(7) Sheinker, V. N.; Movshovich, D. Y.; Osipov, O. A.; Garnovskii, A. D. *Zh. Obshch. Khim.* **1973**, *43*, 2725.
(8) Zimmerman, H. *Z. Electrochem.* **1961**, *65*, 821.
(9) Wolff, H.; Wolff, E. *Spectrochim. Acta, Part A* **1971**, *27a*, 2109.
(10) Wolff, H.; Muller, H. *J. Chem. Phys.* **1974**, *60*, 2938.

SANS and SAXS Studies on Molecular Conformation of a Block Polymer in Microdomain Space

Hirokazu Hasegawa, Takeji Hashimoto,* and Hiromichi Kawai[†]

Department of Polymer Chemistry, Kyoto University, Kyoto 606, Japan

Timothy P. Lodge,[‡] **Eric J. Amis,**[§] **Charles J. Glinka, and Charles C. Han***

Center for Materials Science, National Measurement Laboratory, National Bureau of Standards, Washington, D.C. 20234. *Received March 26, 1984*

ABSTRACT: The molecular conformation of a block polymer chain in a microphase-separated domain space (a confined space) was studied by small-angle neutron scattering (SANS) with a deuterium labeling technique. The samples studied were polystyrene–polyisoprene diblock polymers, and they have a morphology of highly oriented alternating lamellar microdomains composed of polystyrene (PS) and polyisoprene (PI) in bulk when cast from dilute solutions in toluene. Small-angle X-ray scattering (SAXS) measurements were conducted on the same specimens used for SANS in order to separate the scattering arising from a single chain $P(q)$ and that arising from the microdomain structure $S(q)$. Components of the radius of gyration of the single deuterated PS chain in PS lamellae, parallel (R_{gx} or R_{gy}) or perpendicular (R_{gz}) to the interfaces between the two microdomains, were determined with the high-concentration labeling technique of SANS coupled with the SAXS technique. The results indicated that (i) the chain is expanded normal to the interfaces, giving rise to $R_{gz} \simeq 1.6R_{gx}$, (ii) the chain is contracted parallel to the interfaces, giving rise to $R_{gx} \simeq 0.7R_{gx,0}$ ($R_{gx,0}$ being a component of the radius of gyration of the corresponding unperturbed chain), and (iii) the longitudinal expansion is compensated by the lateral contraction, giving rise to an overall radius of gyration R_g nearly equal to or slightly less than R_{g0} for the unperturbed chain. Conclusion (iii) does not mean at all that the chains in domain space are unperturbed but rather that they are strongly perturbed. The lateral contraction was proposed to be the consequence of the repulsive potential between the centers of block chains which are located in narrow interfacial regions (i.e., essentially in the two-dimensional space). A residual "memory" of the repulsion in the bulk block polymer could be a consequence of the two-dimensionality of the space available to chemical junctions of the block polymers and/or an effect of repulsive potential (which existed in the polymer solution with a good solvent) being "locked-in" at high polymer concentrations.

I. Introduction

It is well-known that block polymers (e.g., AB) adopt a microdomain structure in the strong segregation regime for which $\chi Z \gg (\chi Z)_c$, where χ is the Flory–Huggins interaction parameter between the constituent polymers A and B, Z is the total degree of polymerization of the AB diblock polymer, and $(\chi Z)_c$ is the critical value of χ.[1-15] In this regime, A (B) polymers segregate themselves into A (B) microdomains with their chemical junction points being localized in narrow interfacial regions (Figure 1).[3,9,10,13,14,16-25] The "characteristic interfacial thickness"[9] is reported to be about equal to or less than 2 nm for polystyrene–polyisoprene (SI) or polystyrene–poly-

[†] Current address: Hyogo University of Education, Yashiro-cho, Kato-gun, Hyogo-Ken, Japan.
[‡] Current address: Department of Chemistry, University of Minnesota, Minneapolis, MN 55455.
[§] Current address: Department of Chemistry, University of Wisconsin, Madison, WI 53706.

0024-9297/85/2218-0067$01.50/0

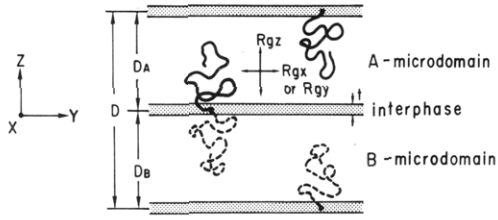

Figure 1. Schematic diagram showing the segregated lamellar microdomain structure of an AB diblock polymer. A (B)-block chains are confined in the A (B) microdomain of thickness D_A (D_B) and the chemical junction points of the A and B chains are confined in the narrow interfacial regions (defined as "interphase") of thickness t. The z component of the radius of gyration of a block chain (z axis being normal to the interface) is designated by R_{gz} and the x (y) component (x (y) axis being parallel to the interface) by R_{gx} (R_{gy}).

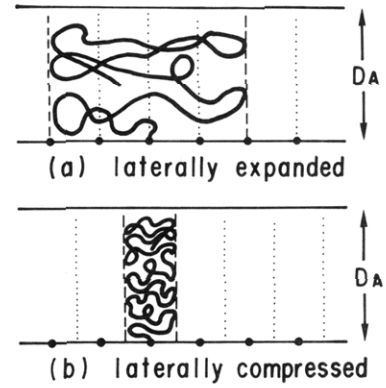

Figure 2. Schematic diagram showing two extreme cases of lateral chain dimensions: (a) the chain is laterally exanded; (b) the chain is laterally compressed. Domain size D_A, mass density ρ_{A0}, and the surface density of block polymer N/S are the same for the two cases.

butadiene (SB) diblock polymers in bulk at room temperature.

Owing to the strong segregation effect between A and B, an A-block chain should have one end in the interphase (i.e., the interfacial region with a finite thickness) and all its segments confined in the A microdomain ("constraint-volume effect"). Furthermore, due to the incompressibility of polymeric liquids, the A chain should have conformations satisfying the requirement of "uniform space filling" with the segments. These two factors, the constraint-volume effect and the uniform space-filling effect, clearly perturb the conformation of the chains in the domain space along the z direction, i.e., the direction normal to the interfaces, relative to the pure homopolymer conformation. The equilibrium perturbation of a chain and its relationship with the domain size, D_A, D_B, and D, have been extensively studied theoretically by Meier,[3,25] by Helfand,[9,10] and recently by Noolandi and Hong.[12,13] Critical tests of the theories have been made by Hashimoto et al.,[20-22] Hadziioannou and Skoulios,[26] and Richard and Thomason,[27] the results of which indicate a satisfactory agreement between theoretical and experimental results. DiMarzio et al.[28] further extended the theory for block polymers to the case where one block forms a crystalline microdomain.

All these theories assume no lateral perturbation of the chains; i.e., the average chain dimensions are unperturbed along the x and y directions. The validity of this assumption cannot be unequivocally tested by experimental determination of the domain size D_K (K = A or B) or D. This is because the lateral chain perturbation is essentially independent of the domain size D_K and D. To make this point clear, consider two extreme cases as depicted in Figure 2, (a) the case where the chain is laterally expanded and (b) the case where the chain is laterally compressed. Even in these two cases, the microdomain A can have a given domain size D_A and mass density ρ_{A0} (which is identical with that of homopolymer A in bulk) as long as the surface density of the block polymer, N/S, satisfies eq I-1, N being the number of block polymer chains per interfacial area S

$$D_A = 2(N/S)\bar{v}_A \qquad \text{(I-1)}$$

$$\bar{v}_A = M_A/(\rho_{A0}N_A)$$

where $\bar{v}_A$ and M_A are, respectively, the molecular volume and the molecular weight of an A-block chain and N_A is Avogadro's number. Since the surface density of the block polymer chain is identical in both cases, the above two cases differ from each other only in terms of segmental overlap or interpenetration in lateral directions; clearly case a involves a much greater degree of segmental overlap than case b. Consequently the lateral chain perturbation is generally independent of the longitudinal chain perturbation, and the lateral perturbation does not need to be considered when one is interested only in domain size and interfacial thickness. However, for better understanding of microdomain structure and hence of microphase separation, one needs the information on the conformation of a block chain in the "microdomain space" relative to that in "free space", free in a sense that there is no constraint-volume effect. The lateral chain perturbation may have an important effect on dynamical properties through molecular entanglements in the microdomain space, because the entanglements should depend on the lateral interpenetration of the chains and hence the lateral chain perturbation. It may also affect the order–disorder transition point, i.e., the point at which the microdomains are dissolved and formed.

Studies on the conformation of a single chain in the domain space are a natural extension of conformational studies in bulk polymers, i.e., studies in free space. They may be pursued by a deuterium labeling technique in small-angle neutron scattering (SANS).[49,55] Hadziioannou et al.[29] first reported such a study for SI diblock polymer having lamellar microdomains and determined the radii of gyration parallel to the interface; the values reported were much smaller than the corresponding unperturbed chain dimensions, with the ratio of the two ranging from 0.78 to 0.67. On the other hand, the radii of gyration of a single block chain in spherical domains were reported to be nearly equal to those of corresponding unperturbed chains for SI diblock polymer[47] and SB diblock polymer.[48] It will be shown in this study that this phenomenon is merely a consequence of the contraction of a chain parallel to the interface being counterbalanced by the expansion of the chain normal to the interface. We will propose that we cannot overlook the strong perturbation of a chain in the domain space from a superficial interpretation of the results with the spherical domain systems (section IV-3).

In the study reported here both $R_{gz,m}$ the radius of gyration normal to the interface, and $R_{gx,m}$, the radius of gyration parallel to the interface, have been measured. Two particular features of this work are worth noting. The labeled block polymer was prepared with a degree of polymerization almost identical with that of the unlabeled block polymer, and it was mixed with the unlabeled block polymer with weight fractions of the labeled polymer being 0.125, 0.25, and 0.50, an amount much greater than that used by Hadziioannou et al. The greater amount of the labeled block polymer mixed in the system should not

affect the intensity distribution of the "molecular scattering", which depends on the conformation of a single chain.[30-32] It would enhance greatly the signal-to-noise ratio of the molecular scattering, however, since its absolute intensity is proportional to $\phi_D(1 - \phi_D)$, ϕ_D being the volume fraction of the labeled chain, and therefore it should provide an improved measurement of the radius of gyration. Small-angle X-ray scattering (SAXS) was also measured from the same specimens used for SANS measurements to separate carefully the contribution due to "molecular scattering" from the net scattering as will be discussed in detail in sections IV-1 and IV-2.

The experimental approach is described in section II, including sample preparation, characterization, and SANS and SAXS optics and techniques. Section III is concerned with experimental results on the morphology of the block polymer studied (section III-1) and SAXS and SANS scattering profiles (sections III-2 and III-3). Some comparisons of SAXS and SANS profiles will be presented in section III-4. Finally section IV is concerned with the extraction of molecular scattering from the net scattering (sections IV-1 and IV-2) and determination and interpretation of the radii of gyration $R_{gx,m}$ and $R_{gz,m}$.

II. Experimental Approach

1. Polymerization and Characterization of Block Polymers. A protonated polystyrene–protonated polyisoprene block polymer (HSI) and a deuterated polystyrene–protonated polyisoprene block polymer (DSI) were synthesized by living anionic polymerization (sequential addition of monomers) with *sec*-butyllithium as the initiator and benzene as the solvent. The deuterated styrene monomer (98+ atom % D) was purchased from Aldrich Chemical Co., Inc. This monomer contained deuterated monobromobenzene and some other substances as impurities which could not be removed completely by the ordinary purification process used for the synthesis of protonated block polymers.[33] These impurities react slowly with polystyryl anion to terminate further propagation, resulting in a broad distribution of molecular weight and composition. Therefore we employed the thorough purification technique proposed by Matsushita et al.[33] The deuterated styrene monomer was further purified by a mixture of (triphenylmethyl)lithium and lithium bromide just before the polymerization.[34] Thus the impurities were essentially completely removed from the monomer.

The polymerizations were planned so that the two block polymers, HSI and DSI, should have exactly the same degree of polymerization and molar composition. However, the molecular characterization of HSI and DSI turned out to show a slight difference. The total number-average molecular weights of HSI and DSI obtained by osmometry were 7.51×10^4 and 7.76×10^4, respectively. The weight fractions of polystyrene and polyisoprene blocks were, respectively, 0.462 and 0.538 for HSI obtained by elemental analysis and 0.522 and 0.475 for DSI estimated from the molecular weight of the deuterated polystyrene precursor. Therefore the degrees of polymerization of polystyrene and polyisoprene block chains are 3.39×10^2 and 5.84×10^2 for HSI and 3.62×10^2 and 5.45×10^2 for DSI, respectively. Although the degrees of polymerization do not exactly match for the two block polymers, the difference is less than 7%, which was deemed to be satisfactory for use in this study. The polydispersity indices ($\bar{M}_w/\bar{M}_n$) of the block polymers obtained by GPC (relative to polystyrene homopolymers) were 1.05 for HSI and 1.15 for DSI.

2. Film Preparation. HSI and DSI were blended in the ratios 50:50, 75:25, and 87.5:12.5 by weight. Films were obtained by casting the three kinds of blends and pure HSI and DSI from 10 wt % solutions in toluene in Petri dishes. The solvent was evaporated slowly under a toluene vapor atmosphere with the temperature kept constant at 28 °C. The cast films were carefully removed from the Petri dishes and further dried in a vacuum oven at room temperature for more than 1 week. The thicknesses of the films thus obtained were ca. 40 μm. The specimens for electron microscopy and SAXS and SANS measurements were cut from the same pieces of films. Henceforth the blend samples will be designated 50/50, 75/25, and 87.5/12.5.

3. SANS Measurements. The NBS small-angle neutron scattering instrument[35,36] was used for these measurements. Thermal neutrons from the steady-state NBS reactor are filtered by a liquid-nitrogen-cooled bismuth–beryllium filter to remove core γ-rays and fast neutrons before being monochromated by a helical-channel velocity selector. Collimation is achieved through the 4.5-m evacuated flight path with either a two-aperture configuration of 27 and 12 mm or with a nine-aperture configuration,[35] the former being used for "edge radiation" and the latter for "through radiation" (see Figure 8) in this experiment. Wavelengths of 6.0 and 5.6 Å were used, respectively. The evacuated sample-to-detector distance is 3.6 m. The detector is a Borkowski–Kopp type[37] 65 × 65 cm² two-dimensional detector with an electric resolution of 5 mm (128 × 128 channels) and a spatial resolution of 8 mm. A dedicated DEC 11/23 minicomputer was used to process signals from the detector, to control the spectrometer and the automatic sample changer, and to provide real-time imaging of the data. Complete data sets were transferred to a DEC VAX 11/780 through a direct link. A Ramtek color graphics system was used in conjunction with the VAX computer for interactive data analysis.

4. SAXS Measurements. A Rigaku Denki Rotaflex Ru-Z rotating-anode X-ray generator with a copper target and a Rigaku Denki step-scan goniometer with a scintillation counter were used to obtain SAXS intensity profiles. A slit collimation system was employed, and corrections for the collimation error were performed when necessary. The intensity data were corrected for sample absorption and background scattering and were normalized for the sample thickness. They were also normalized to the scattering intensity of Lupolen, a standard sample used to correct fluctuations in the X-ray source intensity.

III. Results

1. Morphology. Figure 3 shows the morphology of microdomains observed for as-cast films of the deuterated (DSI) and nondeuterated (HSI) block polymers and one of their blends (50/50). The as-cast films were stained by osmium tetraoxide, ultramicrotomed into thin sections, and observed by transmission electron microscopy. They have alternating lamellar microdomains of polyisoprene (dark regions) and polystyrene (bright regions). The spacings and long-range order of these three specimens are almost idenical as is the case for the other blends (75/25 and 87.5/12.5) not shown here.

2. SAXS Profile. The degree of macroscopic orientation of the lamellar microdomains of HSI, DSI, and their blends and their long-range order were examined by SAXS. The SAXS profiles were investigated with a stack of as-cast film specimens about 40 μm thick by irradiating the incident X-ray beam parallel both to the film normal ("through radiation") and to the film surfaces ("edge radiation"). The scattering patterns obtained with a pinhole collimation of the beam and with edge radiation showed strong multiple-order diffraction maxima in a direction normal to the film surfaces as shown in a previous paper (see Figures 4 and 5 in ref 20), indicating a very high degree of lamellar orientation with the interfaces parallel to the film surfaces. For the through radiation the scattered intensity was weak and the profile was circularly symmetric around the incident beam, indicating a random orientation of the lamellae with respect to the film normal.

The scattering profiles were measured more quantitatively with a slit collimation. Figure 4a shows desmeared scattering profiles for the through radiation and Figure 4b shows the scattering profiles along the film normal with the edge radiation.[38]

By comparing parts a and b of Figure 4 for HSI, DSI, and their blends, it is clear that the scattered intensity of the edge radiation is much higher than that of the through radiation by about 1–2 orders of magnitude. This implies that the fraction of lamellae with their normals parallel to the film surface is only about $^1/_{10}$ to $^1/_{100}$ of that of

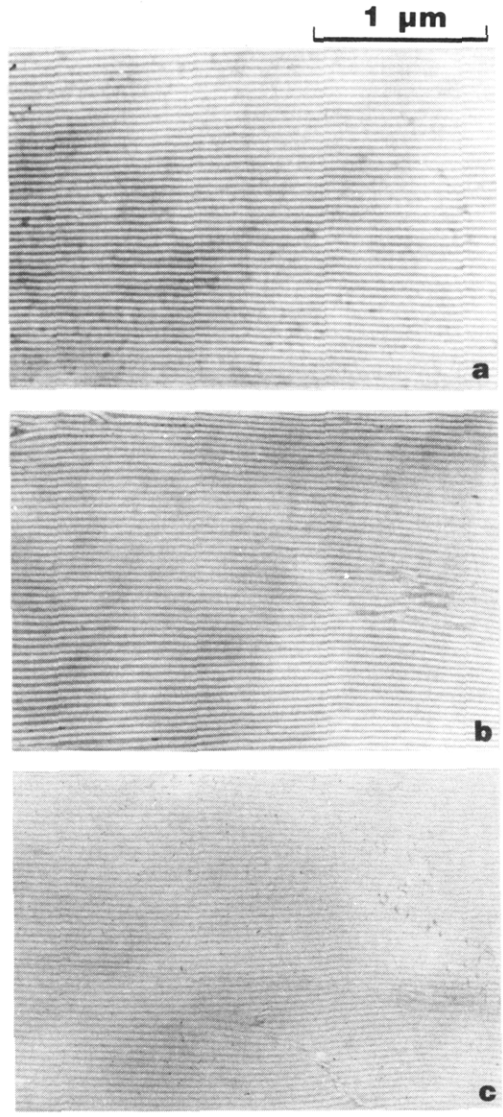

Figure 3. Electron micrographs of (a) DSI, (b) HSI, and (c) 50/50 films, ultramicrotomed normal to the film surfaces, stained with OsO_4. The lamellar interfaces are parallel to the film surfaces.

lamellae with their normals perpendicular to the film surface, indicating a very high degree of planar orientation of lamellae in the solvent-cast films, as found in earlier works.[20,21] The SAXS maxima shown in Figure 4a represent the maxima from the small fraction of lamellae with their normals oriented parallel to the film surfaces; the maxima of each specimen correspond to the first- and third-order peaks from the corresponding lamellar spacing.

The block polymers HSI and DSI and their mixture have a long-range order as shown in Figure 4b. They have almost identical long-range order, spacing, and macroscopic orientation. The paracrystalline disorder of the spacing may be characterized by the g factor, defined by $g = \Delta D/\bar{D}$, where ΔD is the fluctuation of the spacing from the average $\bar{D}$. According the Hosemann and Baguchi,[39] if an nth-order maximum is distinguishable from the background but the $(n + 1)$th order is not, then

$$0.35/(n + 1) \lesssim g \lesssim 0.35/n \qquad \text{(III-1)}$$

Since the profiles for the edge radiation show at least an eighth-order maximum, in this case $0.04 \lesssim g \lesssim 0.044$. In Figure 4b, each profile shows that the intensity of the even-order peaks is much less than that of the odd-order peaks, indicating that the volume fraction of each microdomain is almost identical.[19] For this particular case, the

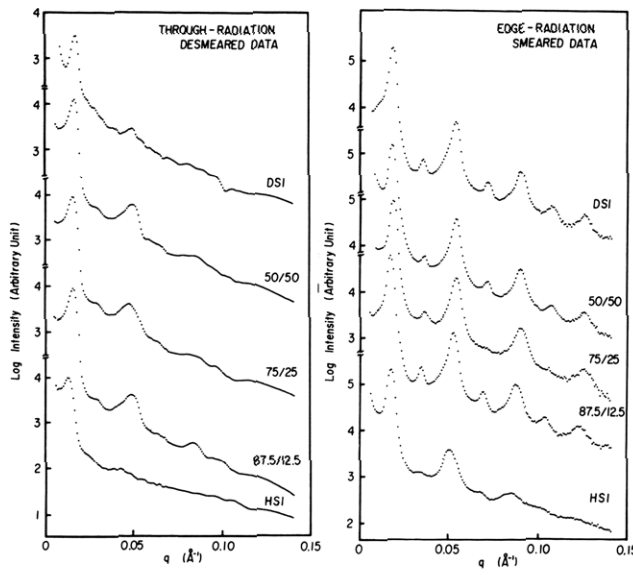

Figure 4. SAXS profiles of DSI, 50/50, 75/25, 87.5/12.5 and HSI (a) measured with through radiation, corrected for the collimation errors, and (b) measured with edge radiation.

scattered intensity from an individual lamella becomes almost negligible at the scattering angles where the lattice factor shows the even-order peaks, as will be discussed in section III-4.

3. SANS. Figure 5 shows contour patterns for SANS from the mixtures of HSI and DSI as well as those from pure block polymers HSI and DSI. These patterns were taken with the edge radiation in which the film normals are in the vertical direction of Figure 5. The circles in the centers of the patterns are zero-intensity regions due to the fixed beamstop on the detector. The beam center was shifted toward the left side of the detector. Each sample shows strong scattering normal to the film surface, indicating again that a high degree of lamellar orientation exists with the lamellar normals parallel to the film normal. The block polymer DSI naturally has the strongest scattering power because of the greater contrast between the domains composed of pure deuterated polystyrene and protonated polyisoprene. It should be noted that even in the nondeuterated block polymer HSI the scattering maxima arising from the microdomains appear.

Although all the SAXS profiles and the SANS profiles from DSI and HSI contain information only on the scattering from microdomains, the SANS profiles for the mixtures contain information on the molecular scattering from individual deuterated polystyrene chains as well. The scattering profiles along $\Phi = 90°$ and $0°$ are shown in Figure 6, parts a and b, respectively, where Φ is the azimuthal angle of the scatering vector $\mathbf{q}$ for edge radiation as defined in Figures 5 and 8b. These profiles were corrected for electronic background, air scattering, sample transmission, and sample thickness and were normalized to the same total number of incident neutrons. The intensity was sector averaged for the same q over an azimuthal angular range of 10°, q being the magnitude of the scattering vector defined by

$$q = 2\pi s \qquad \text{(III-2)}$$

$$s = 2(\sin\theta)/\lambda$$

where 2θ is the scattering angle and λ is the wavelength. As in the SAXS profiles the multiple-order diffraction maxima are observed at the scattering angles satisfying the Bragg condition

$$sD = n \qquad (n = 1, 2, \ldots) \qquad \text{(III-3)}$$

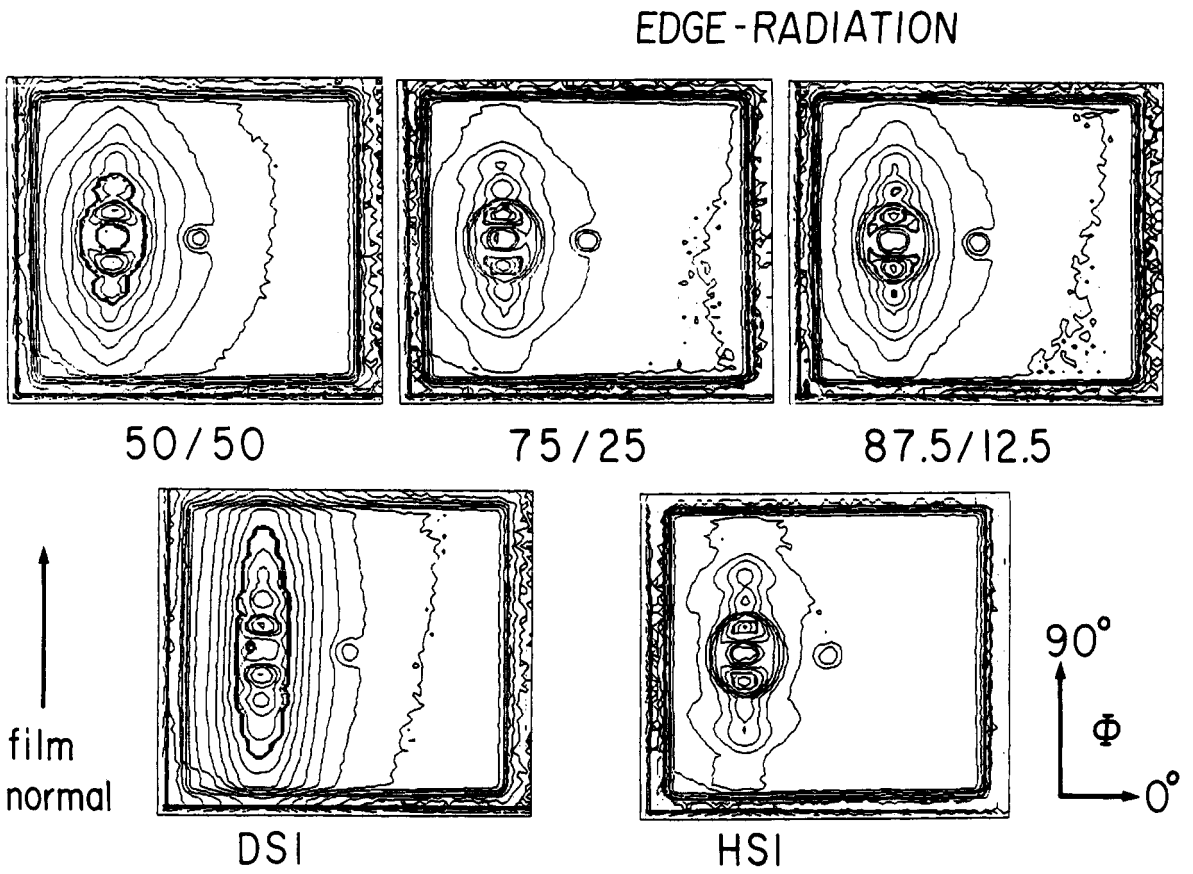

Figure 5. SANS contour patterns of 50/50, 75/25, 87.5/12.5, DSI, and HSI taken with edge radiation. The film normals are in the vertical direction of the patterns. The definition of the azimuthal angle Φ is shown by the arrows. The beam center was shifted toward the left side in each pattern.

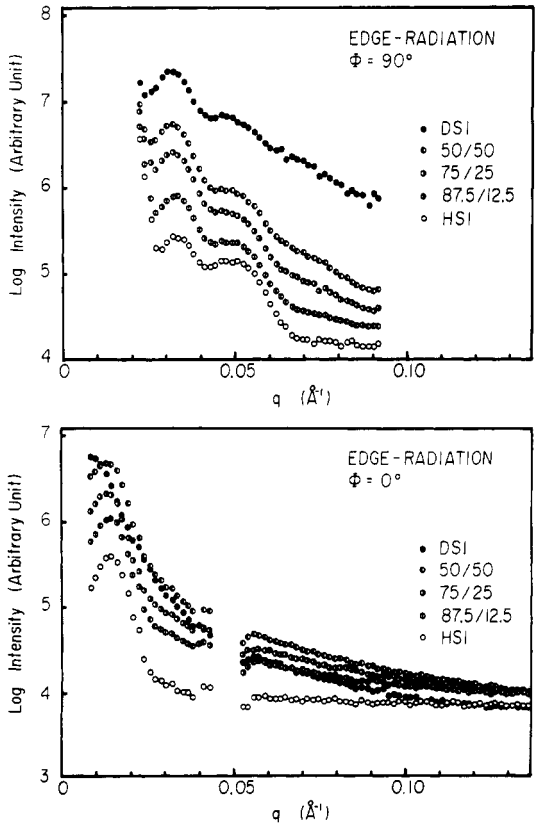

Figure 6. SANS profiles of DSI, 50/50, 75/25, 87.5/12.5, and HSI with the edge radiation (a) along Φ = 90° and (b) along Φ = 0° obtained by averaging in intensity data for the sectors of ΔΦ = 10°. The discontinuous part for Φ = 0° is due to the beamstop fixed on the detector.

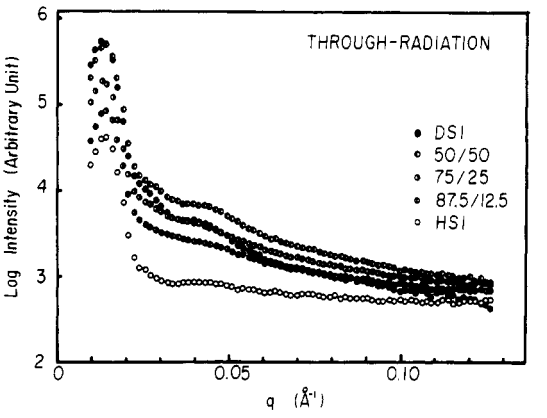

Figure 7. SANS profiles of DSI, 50/50, 75/25, 87.5/12.5, and HSI obtained with through radiation by circular averaging.

where $D = D_A + D_B$, the identity period of the lamellar microdomains.

The scattered intensity at Φ = 0° is much lower than that at Φ = 90°, by about 2 orders of magnitude as found in the SAXS data, which again indicates a very high degree of lamellar orientation. Figure 7 shows the scattering profiles obtained with through radiation. The intensity level of the scattering taken with the through radiation is not identical with that of the scattering at Φ = 0° taken with the edge radiation because of the difference of the optical arrangement as described in section II-2. However, if the difference in the optical system is taken into account, the intensity levels of the scattering profiles shown in Figures 6b and 7 become almost identical, indicating uniaxially symmetric orientation distribution of the lamellar normals with respect to the film normal.

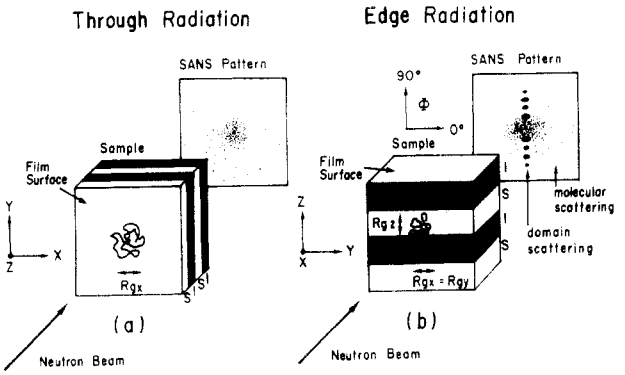

Figure 8. Schematic diagram of the geometry of the samples (perfectly oriented lamellae) and the SANS patterns for (a) the through radiation and (b) the edge radiation. The white microdomains represent the polystyrene phase and the black ones represent the polyisoprene phase. The molecular scattering is indicated by small dots and the domain scattering by large spots in the SANS patterns. The azimuthal angle Φ is also defined in the diagram.

Table I
Bragg Spacings (Edge Radiation at Φ = 90°) (Å) of DSI, HSI, and Their Blends Measured by SAXS and SANS

	DSI	50/50	75/75	87.5/12.5	HSI
SAXS	400	400	400	410	420
SANS	410	400	400	390	380

Figure 8 illustrates schematically the relative contribution of the scattering due to the microdomain structure, designated as "domain scattering", and that due to the conformational characteristics of the deuterated polystyrene block chains, designated as "molecular scattering", to the total scattering. When the radiation is incident along the x direction, parallel to the film surface, the domain scattering occurs normal to the domain boundary and gives rise to a series of multiple-order Bragg diffraction peaks along the z direction as shown in Figure 8b, if the microdomains are macroscopically oriented with their normals parallel to the z direction (see Figure 8b). Superposed on this strong domain scattering is a diffuse molecular scattering which may be elongated parallel to the y axis if the radius of gyration of the polystyrene block in the z direction (R_{gz}) is larger than that in the y direction (R_{gy}) ($R_{gx} = R_{gy}$). When the incident beam is normal to the interface, i.e., along the z direction, and if the domains are perfectly oriented as shown in Figure 8a, the molecular scattering will make the most significant contribution, and its angular dependence is related to the radii of gyration of the polystyrene block in the plane normal to the scattering vector **q**, i.e., R_{gx} and R_{gy}.

4. Discussion. In this section the SAXS and SANS profiles measured on the same specimens are compared qualitatively. Both SAXS and SANS profiles, especially for the edge radiation and the profiles along Φ = 90°, show multiple-order diffraction from a single identity period D of the alternating lamellar microdomains. The spacings measured from SAXS and SANS are identical within the experimental error as shown in Table I. Both SAXS and SANS results yield an almost identical degree of lamellar orientation for a given specimen, a very high degree of orientation of lamellae with their normals perpendicular to the film surfaces. However, it should be noted that the degree of lamellar orientation varies slightly among the different specimens as may be seen in the variation of the intensity ratios for the SAXS curves taken with through and edge- radiations (Figures 4a,b) among the different specimens. This effect is also seen in the variation of the

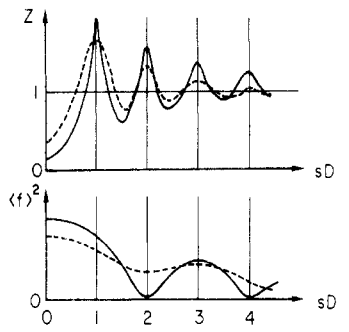

Figure 9. Schematic illustration of the distributions of the lattice scattering factor Z and the particle scattering factor $\langle f \rangle^2$ with the reduced scattering angle sD for the cases of a high-resolution system (solid curves) and low-resolution system (broken curves).

SANS contour patterns for different specimens as shown in Figure 5. It should be noted that the shape of the SANS patterns depends also upon the "effective scattering power" relative to the background scattering arising from incoherent scattering and scattering due to thermal density fluctuations. The power is related to the contrast between the two microdomains.

In the case of SAXS, the scattering profiles of DSI and HSI and their mixtures are identical as long as the microdomain structure is identical. On the other hand, the SANS intensity very much depends on the fraction of deuterated block polymers simply due to the variation of the scattering contrast between the two microdomains as shown in Figure 6 and 7. The SANS profiles for the mixtures of DSI and HSI depend also upon molecular scattering, a contribution of which does not exist in SAXS at all.

The SAXS profiles show a greater number of scattering maxima with smaller peak widths compared with the SANS profiles. These effects result from the SAXS being measured with an incident beam having a much narrower spectral width and with an optical system having a higher spatial resolution in comparison to the SANS measurements.

The difference in the spectral width of the incident beam may account also for the difference in relative peak heights between the SAXS and SANS profiles obtained with edge radiation (see Figures 4b and 6a); the SAXS profiles show even-order peaks being very much depressed in comparison with the odd-order peaks whereas the SANS profiles show rather strong even-order peaks. It should be noted that the two maxima at $q \simeq 0.032$ and 0.047 Å^{-1} in the SANS profiles shown in Figure 6a correspond to the second- and the third-order maxima, respectively. Figure 9 schematically illustrates the reason why the even-order peaks are very much depressed for the alternating lamellae with equal volume fractions of the two microdomains.

The scattered intensity I from a lamellar microdomain system is approximately given by a product of the lattice factor or the interference function Z and the particle scattering factor $\langle f \rangle^2$

$$I \sim \langle f \rangle^2 Z \qquad \text{(III-4)}$$

The particle factor $\langle f \rangle^2$ becomes almost zero at $sD = 2, 4$, etc., where the even-order maxima appear in Z if the particle volume fraction is 0.5,[19] as shown by the solid lines in Figure 9. Hence the even-order diffraction maxima are much weaker than the odd-order diffraction maxima as seen in the SAXS profiles. However, if the spectral distribution of the incident beam is wide, both Z and $\langle f \rangle^2$ may show broader profiles as represented by the broken curves in Figure 9. The particle factor may not necessarily go to

zero at $sD = 2n$ (n an integer), giving rise to much stronger even-order peaks, as seen in the SANS profiles. Hadzioannou et al.[29] attributed the enhancement of the even-order peaks to multiple scattering. The results presented here do not support this interpretation, however, because (a) the transmission of the samples is not very much different between the SAXS and SANS measurements and (b) the relative peak heights are almost identical among DSI, HSI and their mixtures as shown in Figure 6a, despite the fact that the scattering power of these samples varies greatly.

IV. Extraction of Molecular Scattering

1. **Method.** The high-concentration labeling technique has been discussed and used recently.[30-32] In this paper, due to the imperfect orientation of the lamellae a slightly modified treatment has been employed. Figure 8 shows the geometry of the samples and the SANS patterns in the case where the lamellae are perfectly oriented with their normals perpendicular to the film surface. In this situation the observed scattering for the through radiation of the blend films is the sum of the molecular scattering from the deuterated polystyrene block chains and the net incoherent scattering intensity (Figure 8a). Thus, just by subtracting the incoherent scattering intensity from the observed intensity, the molecular scattering can be obtained and the lateral chain dimension in the lamellar microdomain can be determined. However, the scattering peaks seen in Figures 4a and 7 indicate that the orientation of the lamellae is not so perfect as depicted in Figure 8. It is slightly perturbed so that the domain scattering from the lamellae oriented with their normals parallel to the film surface cannot be neglected although their fraction is much smaller than that of the lamellae with their normals perpendicular to the film surface. Therefore the scattering intensity from the blend film should be written as

$$I(q) = \phi_D(1 - \phi_D)(a_H - a_D)^2\phi_{PS}P(q) + S(q) + I_{in} \quad \text{(IV-1)}$$

where ϕ_D is the volume fraction of the deuterated styrene monomer in the polystyrene microdomain, a_H is the scattering length of the protonated styrene monomer unit, a_D is the scattering length of the deuterated styrene monomer unit, $P(q)$ is the molecular scattering function of the polystyrene block chains, and $S(q)$ is the domain scattering function from the lamellae with their normals parallel to the film surface, which depends on ϕ_{PS}, the volume fraction of the polystyrene domain, $(\beta_I - \beta_S)^2$, the difference of the scattering contrast between the respective domains, and the number of lamellae contributing to $S(q)$. β_I and β_S are defined as follows: β_I is the scattering length density of the polyisoprene microdomain and β_S is the scattering length density of the polystyrene microdomain, I_{in} is the net incoherent scattering intensity. The a and β parameters were calculated from the coherent atomic scattering lengths of H, D, and C reported in the literature,[40] the fraction of the deuterated and protonated block polymers, and the density of each microdomain of the block polymers, assuming that the densities of the microdomains do not differ from those of the corresponding homopolymers and also assuming incompressibility on blending.

The SANS scattering of the blend films measured at the azimuthal angle $\Phi = 0°$ with edge radiation should be the same as that with through radiation as shown in Figure 8 and can be treated in the same manner because of uniaxial symmetry in the orientation distribution of lamellae with respect to the film normal. On the other hand, the scattering at $\Phi = 90°$ with edge radiation involves very strong scattering from the lamellar microdomains, within which are located the deuterated polystyrene block chains causing the molecular scattering. In this case formula IV-1 is applicable if $S(q)$ is replaced by the scattering function of the lamellae with their normals oriented perpendicular to the film surface.

a. Evaluation of I_{in}. The incoherent scattering intensity does not depend on the scattering angle while the coherent molecular scattering intensity decays with increasing scattering angle. In Figures 6 and 7 the total scattered intensity $I(q)$ of HSI levels off at high q, while $I(q)$ for the samples containing deuterated polystyrene blocks continues to decrease. This suggest that the coherent scattering intensity of HSI in the high-q region is negligible compared with the incoherent scattering and that the constant intensity values in the high-q region (q = 0.0938–0.1268 Å^{-1} for the through radiation and q = 0.1300–0.1363 Å^{-1} for the edge radiation) can be considered as the I_{in} for HSI. Since the chemical composition of each sample is known, the incoherent scattering power of each sample can be calculated by using reported values of incoherent scattering cross sections for the constituent atoms.[40] Thus I_{in} for each deuterium-containing sample was calculated from the measured values of I_{in} for HSI, according to the ratio of the incoherent scattering power. The same I_{in} values were used for the azimuthal angles $\Phi = 0°$ and $\Phi = 90°$ (edge radiation) because there is no azimuthal angle dependence of I_{in}, and the scattering intensities were obtained simultaneously for the two angles. The coherent scattering curves were obtained by subtracting the values of I_{in} from the net scattering curves.

b. Extraction of Molecular Scattering. The coherent scattering of DSI and HSI consists of domain scattering only. Therefore the scattering function $S(q)$ is known for both DSI and HSI. If the domain structures of the blends and the pure block polymers were identical, $S(q)$ for either DSI or HSI could be substituted into eq IV-1 directly to obtain the molecular scattering. However, in this experiment $S(q)$ varies slightly from sample to sample because of the inevitable small variations in the lamellar microdomain structure, due to the synthesis and film-casting techniques. The change in the domain spacing affects the lattice factor Z in eq III-4, resulting in shifts of the peak positions of the scattering curves. This problem can be easily overcome by handling the scattered intensities as a function of qD, D being the Bragg spacing of the domains, instead of as a function of q. Then the peaks of the scattering curves for different samples should appear at the same positions, i.e., qD = 1, 2, 3, ..., and the subtraction of one scattering curve from another becomes possible.

On the other hand, the change in the volume fraction of the polystyrene and polyisoprene domains will affect the particle scattering factor $\langle f \rangle^2$ in eq III-4 and change the shapes of the scattering curves, e.g., the relative peak heights between the first-order and higher order maxima. In this case the determination of the domain scattering $S(q)$ for the blend of the deuterated and protonated block polymers is not simple. As a first-order approximation additivity of $S(q)$ on blending was assumed. This is not right when the difference in domain structures is great but may be valid when it is very small. Consequently the following equation was used to calculate the domain scattering of the blends, $S_B(qD)$

$$\frac{S_B(qD)}{c_B(\beta_{IB} - \beta_{SB})^2} = (1 - \phi_D)\frac{1}{c_H(\beta_{IH} - \beta_{SH})^2}[I_H(qD) - I_{in,H}] + \phi_D\frac{1}{c_D(\beta_{ID} - \beta_{SD})^2}[I_D(qD) - I_{in,D}] \quad \text{(IV-2)}$$

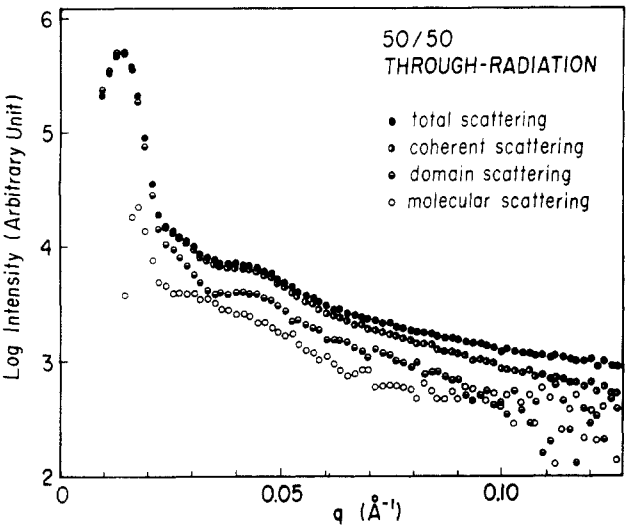

Figure 10. An example showing the process of extracting the molecular scattering from the total SANS function for the 50/50 sample measured with through radiation. Profiles of the total scattering, the coherent scattering, the domain scattering, and the molecular scattering are shown.

where $S_B(qD)$ is the domain scattering function for the blend and $(\beta_{IK} - \beta_{SK})$ (K = B, H, or D) is the difference of the scattering contrast between polyisoprene and polystyrene microdomains, where B, H, and D designate the blends, HSI, and DSI, respectively. The values $(\beta_{IK} - \beta_{SK})$ are calculated as described above. $[I_J(qD) - I_{in,J}]$ (J = H or D) are the domain scattering corrected for the incoherent scattering for HSI and DSI, respectively, which can be measured under through radiation. c_B, c_H, and c_D are the number of lamellae oriented with their normals parallel to the film surfaces for the blends, HSI, and DSI. The ratios c_B/c_H and c_B/c_D can be determined from corresponding intensity ratios for the SAXS maxima measured with through radiation.

The domain scattering function of each blend was calculated by using eq IV-2, and the molecular scattering function for the deuterated polystyrene chains was extracted via eq IV-1. An example of this process is shown in Figure 10 for the through radiation of the 50/50 blend, where curves for the total scattering, $I(q)$, the coherent scattering, $[I(q) - I_{in}]$, the domain scattering, $S(q)$, and the molecular scattering, $P(q)$, are plotted. It should be noted that the molecular scattering and the domain scattering have almost the same order of magnitude in this case. Similar results were obtained for the through radiation of the other blends and for the edge radiation at $\Phi = 0°$ of all three blends. This method is employed also for the edge radiation at $\Phi = 90°$. Since the intensity level of the domain scattering is considerably higher than that of the molecular scattering, due to the highly oriented domain structure, the extracted molecular scattering function may contain much larger errors than those obtained for the through radiation and the edge radiation at $\Phi = 0°$. For the edge radiation at $\Phi = 90°$, $[I_J(qD) - I_{in,J}]$ (J = H or D) are the domain scattering corrected for the incoherent scattering for HSI and DSI, respectively, which can be measured under edge radiation at $\Phi = 90°$. The ratios c_B/c_H and c_B/c_D can be determined from corresponding intensity ratios for the SAXS maxima measured with edge radiation at $\Phi = 90°$.

2. Results. The molecular scattering obtained in section IV-1 is for the anisotropic and oriented block chains. For such a system the Guinier relation[41] between the scattered intensity distribution at $\Phi = 0°$ (or $\Phi = 90°$) and

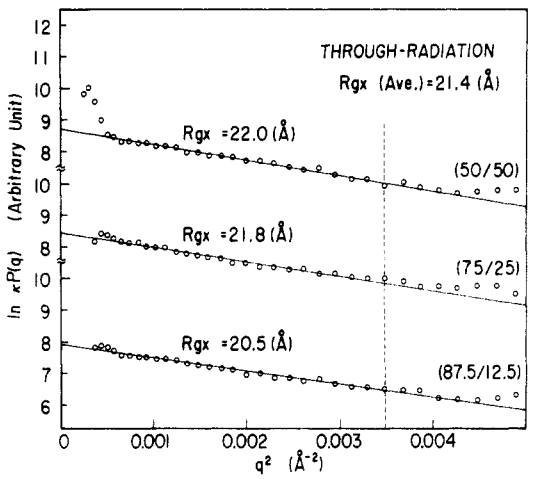

Figure 11. Guinier plots for the molecular scattering of 50/50, 75/25, and 87.5/12.5 obtained with the through radiation. The coefficient κ equals to $\phi_D(1 - \phi_D)(a_H - a_D)^2\phi_{PS}$. The solid straight lines were obtained by the least-squares fit of the data points. The upper limit of q^2 for the Guinier approximation is indicated by the vertical broken line.

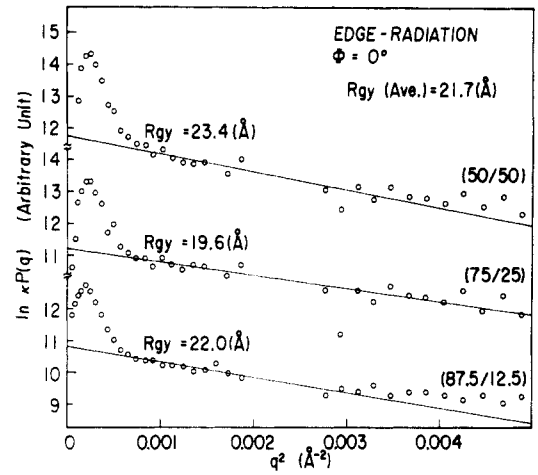

Figure 12. Guinier plots for the molecular scattering of 50/50, 75/25, and 87.5/12.5 obtained with the edge radiation at $\Phi = 0°$. Some data points are missing due to the beamstop fixed on the detector.

the corresponding component of the radius of gyration R_{gy} (or R_{gz}) is given as

$$P(q) \sim \exp(-q^2R_{gy}^2) \qquad (\text{for } \Phi = 0°) \qquad \text{(IV-3)}$$

where R_{gy} is the radius of gyration of the coil with respect to the plane perpendicular to the y axis. Therefore the slope of ln $P(q)$ vs. q^2 gives R_{gy}^2 (Figure 12). For the through radiation the Guinier approximation, eq IV-3, may be valid in the region where $(gR_{gy})^2 \lesssim 1.3^2$ since the segmental distribution of a single block chain projected on the x–y plane (parallel to the lamellar interface) is considered isotropic, and this limit is shown by a vertical broken lin in Figure 11. It should be noted that the limiting value 1.3 was determined for a sphere (see Figure 38 of ref 41) and hence is not a rigorous value for polymer coils but it rather gives an approximate value. Within this limit the plotted curves show reasonably linear regions for each case although there are some residual peaks arising from small errors in the subtraction of the domain scattering. It is clear that $R_{gx} = R_{gy}$ from symmetry considerations.

The slopes of the linear region, hence R_{gx} and R_{gz} were obtained by the least-squares fit within the indicated range but ignoring the data points in the region of the first peak.

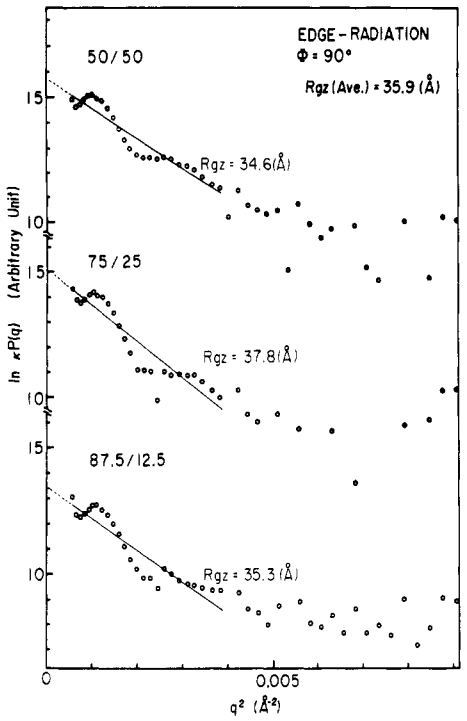

Figure 13. Guinier plots for the molecular scattering of 50/50, 75/25, and 87.5/12.5 obtained with the edge radiation at $\Phi = 90°$. The range of q^2 for the least-squares fit is indicated by the solid lines.

Table II
Comparison of Experimental and Theoretical Values of $P(q = 0,\phi_D)/P(q = 0,\phi_D = 0.5)$

		exptl			
sample	ϕ_D	through	edge, $\Phi = 0°$	edge, $\Phi = 90°$	theor
87.5/12.5	0.117	0.45	0.39	0.10	0.414
75/25	0.237	0.79	0.58	0.50	0.724

Significant nonlinear character remains in the Guinier plot of the edge radiation data at $\Phi = 90°$. Because of the extremely strong domain scattering, any slight mismatch between the real domain scattering function and the domain scattering function calculated from the pure block polymer data could result in a significant distortion in the curve. If the estimation of the magnitude of the domain scattering is correct, however, the resulting curve after smoothing may reasonably represent the molecular scattering. In fact there do seem to be reasonably linear regions with similar slopes for different blends as shown in Figure 13. The slopes thus obtained were used to calculate R_{gz}.

The values of R_{gx} and R_{gz} thus obtained are shown in Figures 11–13. Within experimental error these values show no dependence on the deuterated polystyrene chain concentration and good agreement between R_{gx} obtained from the through-radiation data and that obtained from the edge-radiation data at $\Phi = 0°$.

It is appropriate to test whether the straight lines drawn in Figures 11–13 are reasonable or not. According to eq IV-1, $P(q)$ is proportional to $\phi_D(1 - \Phi_D)$, the product of the fractions of the two components in the blend. Therefore the intensity at the $q = 0$ intercept of each straight line in Figures 11–13, $P(q = 0, \Phi_D)$, should be proportional to $\Phi_D(1 - \Phi_D)$ if they are correct. Table II lists the results of $P(q = 0, \Phi_D)/P(q = 0, \Phi_D = 0.5)$ measured from the through radiation and edge radiation at $\phi = 0°$ and $\phi = 90°$ and those determined from the theoretical considerations. It may be clear that the measured values for both

Table III
Radius of Gyration of Polystyrene Block Chain in the Domain Space

sample	$(\bar{M}_n)_{DPS} \times 10^{-3}$	R_{gx}, Å		$R_{gx,m}/R_{gx,0}$	$R_{gz,m}$	remarks
		$R_{gx,m}$	$R_{gx,0}$			
DSI	40.5	22 ± 1	30	0.71	36 ± 2	this work
SDI-7	68.9	30.8	39.3	0.78		ref 29
SDI-12	110.7	33.6	49.9	0.67		ref 29

the through radiation and the edge radiation at $\phi = 0°$ are in good agreement with the theoretical values but that those for the edge radiation at $\phi = 90°$ are not in satisfactory agreement with the theoretical values. Thus the straight lines drawn in Figures 11 and 12 are reasonable in view of relative intensity level also, but those in Figure 13 are less reliable, again reflecting the difficulty of extracting the molecular scattering.

3. Discussion. In Table III the measured x and z components of the radii of gyration of a single deuterated polystyrene block chain in the domain space, $R_{gx,m}$ and $R_{gz,m}$ (see Figure 8), the measured values $R_{gx,m}$ reported by Hadziioannou et al.,[29] and the values of $R_{gx,0}$, the x component of the radius of gyration of the unperturbed chain in bulk free space, are listed.

The radius of gyration of a single chain R_g is defined as

$$R_g^2 = \int\int\int dx\,dy\,dz\,(x^2 + y^2 + z^2)\rho(x,y,z) = \int\int\int dx\,dy\,dz\,x^2\rho(x,y,z) + \int\int\int dx\,dy\,dz\,y^2\rho(x,y,z) + \int\int\int dx\,dy\,dz\,z^2\rho(x,y,z) = R_{gx}^2 + R_{gy}^2 + R_{gz}^2 \quad \text{(IV-4)}$$

where $\rho(x,y,z)$ is the segment density and R_{gx} is the radius of gyration of a chain along the x direction; R_{gx} can be measured with the **q** vector parallel to the x direction. For a chain with a spherically symmetric distribution of segments

$$R_{gx}^2 = R_{gy}^2 = R_{gz}^2 = R_g^2/3 \quad \text{(IV-5)}$$

while for a chain with a cylindrically symmetric distribution of segments with respect to z (as in a chain in the domain space)

$$R_{gx}^2 = R_{gy}^2 = R_{g\perp}^2/2 \quad \text{(IV-6)}$$

The values $R_{gx,m}$ and $R_{gz,m}$ are the values of R_{gx} and R_{gy} measured by SANS, while the values $R_{gx,0}$ are calculated from the unperturbed dimensions in free space $R_{g,0}$ for the polystyrene block chains; i.e.

$$(R_{gx,0})^2 = (R_{g,0})^2/3 = (Nl^2)/18 \quad \text{(IV-7)}$$

where Nl^2 is the end-to-end distance given by

$$(Nl^2)^{1/2} = KM^{1/2} \quad \text{(IV-8)}$$

For a polystyrene chain in bulk K is reported to be 0.067 nm by Ballard et al.[42] from neutron scattering experiments.

These experimental results and those by Hadziioannou et al.[29] indicate a significant amount of contraction of the lateral dimension of the chain in the domain space in comparison with the dimension of the chain in free space, the ratio $R_{gx,m}/R_{gx,0}$ being about 0.7. In this work the values of $R_{gx,m}$ from the SANS profiles taken with through radiation and edge radiation at $\Phi = 0°$ are in good agreement, while Hadziioannou et al. measured the SANS profiles in the through radiation only.

As far as we are aware, these results also represent the first attempt to measure the longitudinal dimension $R_{gz,m}$, although the accuracy in determining $R_{gz,m}$ is less than that in determining $R_{gx,m}$ owing to the difficulty of extracting the molecular scattering from the total scattering with edge

radiation at $\Phi = 90°$.[43] The value $R_{gz,m}$ thus obtained is much larger than $R_{gx,m}$

$$R_{gz,m} \simeq 1.6R_{gx,m} \quad \text{(IV-9)}$$

and than $R_{gx,0}$, indicating that a strong expansion of the chain along the lamellar normal.

It is worth noting that the overall radius of gyration of the block chain in the domain space R_g is about equal to the overall radius of gyration $R_{g,0}$ of the corresponding unperturbed chain in the free space, since

$$R_g^2 = 2 \times 22^2 + 36^2 \simeq 2.3 \times 10^3 \text{ (Å}^2\text{)}$$

$$R_{g,0}^2 = 3 \times 30^2 = 2.7 \times 10^3 \text{ (Å}^2\text{)} \quad \text{(IV-10)}$$

Thus it appears that the lateral contraction is compensated by the longitudinal expansion. From the lateral contraction only, Hadziioannou et al.[29] suggested two models for the conformation of the chain: (i) random coils stretched along the normal to the interfaces and (ii) the chain confined to a thin, compact, wormlike tube (see Figure 7 of ref 29). The former possibility is first considered below. For simplicity consider a case in which a sphere of radius R (having the radius of gyration R_{gs}) is affinely deformed under constant volume to a spheroid having principal axes $\lambda^{-1/2}R$, $\lambda^{-1/2}R$, and λR, where λ is the elongation ratio. The deformation involves lateral contraction (by a factor $\lambda^{-1/2}$) and longitudinal stretching (by a factor of λ). The radius of gyration of the spheroid R_{ge} is given by

$$R_{ge} = R[(2 + \lambda^3)/5]^{1/2}, \qquad R_{gs} = R(3/5)^{1/2} \quad \text{(IV-11)}$$

$$R_{ge}/R_{gs} = [(2 + \lambda^3)/3]^{1/2} \quad \text{(IV-12)}$$

It is clear that eq IV-12 can be applied also for a deformed random coil. Thus the isochoric and affine deformation involves an increase in the radius of gyration with an increase in the stretching λ; this is not the case for a system in which the overall radius of gyration of the chain R_g is approximately equal to or even less than that of the corresponding unperturbed chain, $R_{g,0}$. Thus the overall radius of gyration of a chain in the domain space appears to be smaller than the radius of gyration of a chain which is stretched affinely under constant volume from an initially unperturbed coil, which, in turn, apparently reflects a genuine lateral contraction of the chain. In other words, the stretching of the random coil chain along the lamellar normal cannot by itself account for the amount of lateral contraction observed in the experiments.

We do not feel it necessary to invoke a particular conformation confined in a wormlike tubes (model ii as described above) to account for the lateral contraction. Rather the lateral contraction simply suggests the existence of a repulsive interaction between the chains in the domain space, i.e., between the chemical junctions of constituent block chains (or approximately between the coil center of block polymer molecules) which are confined in the narrow interfacial region. This point may be further analyzed from an asymptotic behavior of $P(q)$ at large q.

Consider an asymptotic behavior of $P(q)$ at high q for the scattering profile obtained by the through radiation (Figure 14). For a Gaussian chain, it will decrease according to[44-46]

$$P(q) \sim q^{-2} \quad \text{(IV-13)}$$

For a chain with excluded volume[45,46]

$$P(q) \sim q^{-5/3} \quad \text{(IV-14)}$$

For a collapsed chain[45]

$$P(q) \sim q^{-3} \quad \text{(IV-15)}$$

All the molecular scattering profiles obtained experimentally exhibit the asymptotic behavior between those of the ideal Gaussian and excluded-volume chain; i.e., $P(q) \sim q^n$ with $-2 \leq n \leq -5/3$. The behavior is far from that expected for a collapsed chain.

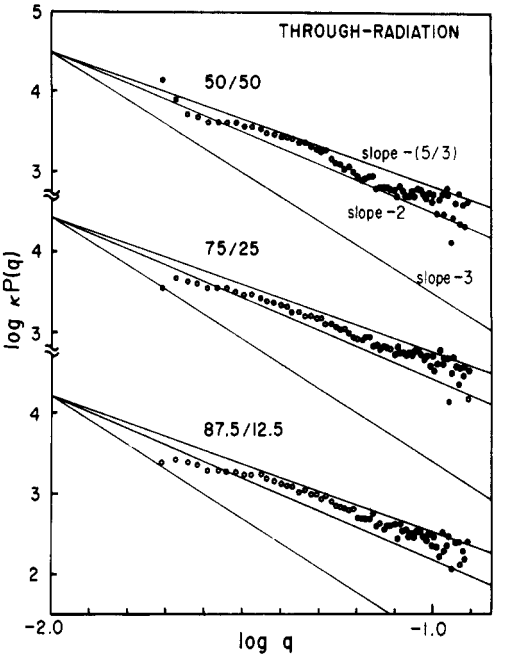

Figure 14. Logarithmic plots of the molecular scattering vs. q for 50/50, 75/25, and 87.5/12.5 obtained with the through radiation. Lines with the slopes of $-5/3$ (for a chain with the excluded volume), -2 (for a Gaussian chain), and -3 (for a collapsed chain) are drawn for comparison.

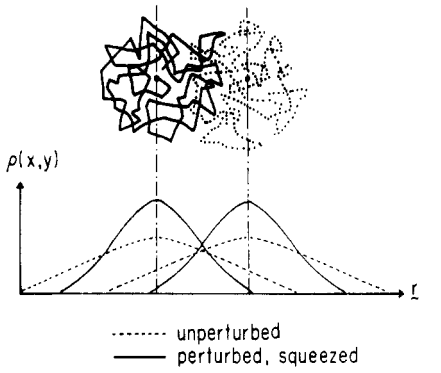

Figure 15. Schematic showing the spatial distribution of segments in the plane parallel to the interface for the neighboring two polymers. The dotted distribution curves $\rho(x,y)$ represent unperturbed chains. The perturbed and squeezed chains illustrated above have the narrower spatial segment density distribution about the center of the molecule as shown by the solid curves.

Figure 15 represents schematically the spatial distribution of segments for the neighboring two polymers in a direction parallel to the interface, i.e., the xy plane in Figure 8. If the lateral dimension is unperturbed, the segments from different polymers can freely interpenetrate, and the spatial distribution of the polymer centers is uniform. The repulsive potential between the neighboring polymers would tend to create a short-range liquid-like order in the spatial distribution of the polymer coil centers in the two-dimensional plane associated with the narrow interface, and the segment density distribution about the center of molecule tends to be compressed, resulting in a lateral contraction.

Polymer chains in bulk are known to be unperturbed, and therefore repulsive interactions between polymers do

not exist. In contrast, the block chains in bulk and in domain space are in a repulsive potential field, although its origin is not well understood at present. The chains in bulk homopolymer are in three-dimensional free space ("free" in the sense of not being confined in domain space). On the other hand, the centers of the block chains in domain space are confined to the two-dimensional space associated with the narrow interphase, with a characteristic interfacial thickness much smaller than the polymer dimension. Thus the dimensionality might be one factor responsible for the enhanced repulsion for the chain in the domain space. Besides the dimensionality, there may be another factor associated with the history of microdomain formation. The microdomains are formed by solvent-casting from dilute block polymer solutions in a good solvent. The repulsive potential between the polymers which exists in dilute and semidilute solutions usually decreases with increasing polymer concentration and vanishes in bulk pure polymer. In the case of the block polymer any short-range liquid-like order which may exist in the solution due to a repulsive potential could be "locked in" at a particular polymer concentration, leading to a residual "memory" of the repulsion in the bulk block polymer.

The lateral perturbation of the block chain in the domain space should tend to increase the free energy of the microdomain, resulting in less stable microdomains. This may then lower the temperature and increase the concentration of the order–disorder transition of block polymers (the transition[11,13-15] which involves dissolution and reformation of the microdomains). However, this may not significantly affect the equilibrium domain size D_A, D_B, and D.

Acknowledgment. We thank Professor T. Fujimoto, Department of Material Science and Technology, Technical University of Nagaoka, Nagaoka, Niigata, Japan, for a suggestion on a purification method of the monomers in the living anionic polymerization of the deuterated block polymer.

Registry No. (Isoprene)·(styrene) (copolymer), 25038-32-8.

References and Notes

(1) Skoulios, A.; Finaz, G.; Parrod, J. *C. R. Hebd. Seances Acad. Sci.* **1960**, *251*, 739. Skoulios, A.; Finaz, G. *Ibid.* **1961**, *252*, 3467. Finaz, G.; Skoulios, A.; Sadron, C. *Ibid.* **1961**, *253*, 265.
(2) Vanzo, E. *J. Polym. Sci., Part A-1* **1966**, *4*, 1727.
(3) Meier, D. J. *J. Polym. Sci., Part C* **1969**, *26*, 81.
(4) Inoue, T.; Soen, T.; Hashimoto, T.; Kawai, H. *J. Polym. Sci., Part A-2*, **1969**, *7*, 1283.
(5) Molau, G. E. In "Block Polymers"; Aggarwal, S. L., Ed.; Plenum Press: New York, 1970.
(6) Hoffmann, M.; Kämpf, G.; Krömer, H.; Pampus, G. *Adv. Chem. Ser.* **1971**, *No. 99*, 351.
(7) Sadron, C.; Gallot, B. *Makromol. Chem.* **1973**, *164*, 301.
(8) Meier, D. J. *Org. Coatings Prepr., Am. Chem. Soc.* **1977**, *37* (1), 246.
(9) Helfand, E. *Macromolecules* **1975**, *8*, 552.
(10) Helfand, E.; Wasserman, Z. R. *Macromolecules* **1976**, *9*, 879; **1978**, *11*, 960; **1980**, *13*, 994.
(11) Leibler, L. *Macromolecules* **1980**, *13*, 1602.
(12) Hong, K. M.; Noolandi, J. *Macromolecules* **1980**, *13*, 964; **1981**, *14*, 727; **1981**, *14*, 736.
(13) Noolandi, J.; Hong, K. M. *Ferroelectrics* **1980**, *30*, 117.
(14) Roe, R.-J.; Fishkis, M.; Chang, C. J. *Macromolecules* **1981**, *14*, 1091.
(15) Hashimoto, T.; Shibayama, M.; Kawai, H. *Polym. Prepr., Am. Chem. Soc., Div. Polym. Chem.* **1982**, *23* (1), 21; *Macromolecules* **1983**, *16*, 1093.
(16) Kim, H. *Macromolecules* **1972**, *5*, 594.
(17) Vonk, C. G. *J. Appl. Crystallogr.* **1973**, *6*, 81.
(18) Skoulios, A. In "Block and Graft Copolymers"; Burke, J. J., Weiss, V., Eds.; Syracuse University Press: Syracuse, NY 1973.
(19) Hashimoto, T.; Nagatoshi, K.; Todo, A.; Hasegawa, H.; Kawai, H. *Macromolecules* **1974**, *7*, 364.
(20) Hashimoto, T.; Todo, A.; Itoi, H.; Kawai, H. *Macromolecules* **1977**, *10*, 377.
(21) Hashimoto, T.; Shibayama, M.; Kawai, H. *Macromolecules* **1980**, *13*, 1237.
(22) Hashimoto, T.; Fujimura, M.; Kawai, H. *Macromolecules* **1980**, *13*, 1660.
(23) Fujimura, M.; Hashimoto, H.; Kurahashi, K.; Hashimoto, T.; Kawai, H. *Macromolecules* **1981**, *14*, 1196.
(24) Hashimoto, H.; Fujimura, M.; Hashimoto, T.; Kawai, H. *Macromolecules* **1981**, *14*, 844.
(25) Meier, D. J. *Prepr. Polym. Colloq., Soc. Polym. Sci., Jpn., Kyoto* **1977**, 83.
(26) Hadziioannou, G.; Skoulios, A. *Macromolecules* **1982**, *15*, 267.
(27) Richard, R. W.; Thomason, J. L. *Macromolecules* **1983**, *16*, 982.
(28) DiMarzio, E.; Guttman, C.; Hoffman, J. *Macromolecules* **1980**, *13*, 1194.
(29) Hadziioannou, G.; Picot, C.; Skoulios, A.; Ionescu, M.-L.; Mathis, A.; Duplessix, R.; Gallot, Y.; Lingelser, J.-P. *Macromolecules* **1982**, *15*, 263.
(30) Williams, C. E.; Nierlich, M.; Cotton, J. P.; Jannink, G.; Boue, F.; Daoud, M.; Farnoux, B.; Picot, C.; de Gennes, P.-G.; Rinaudo, M.; Moan, M.; Wolff, C. *J. Polym. Sci., Polym. Lett. Ed.* **1979**, *17*, 379.
(31) Akcasu, A. Z.; Summerfield, G. C.; Jahshan, S. N.; Han, C. C.; Kim, C. Y.; Yu, H. *J. Polym. Sci., Polym. Phys. Ed.* **1980**, *18*, 863.
(32) Koberstein, J. *J. Polym. Sci., Polym. Phys. Ed.* **1982**, *20*, 593.
(33) Matsushita, Y.; Furuhashi, H.; Choshi, H.; Noda, I.; Nagasawa, M.; Fujimoto, T.; Han, C. C. *Polym. J.* **1982**, *14*, 489.
(34) Fujimoto, T. (Department of Material Science and Technology, Technical University of Nagaoka, Nagaoka, Niigata, Japan), personal communication.
(35) Glinka, C. J. *AIP Conf. Proc.* **1981**, *No. 89*, 395.
(36) Amis, E. J.; Glinka, C. J.; Han, C. C.; Hasegawa, H.; Hashimoto, T.; Lodge, T. P.; Matsushita, Y. *Polym. Prepr., Am. Cehm. Soc., Div. Polym. Chem.* **1983**, *24* (2), 215.
(37) Borkowski, C. J.; Kopp, M. K. *Rev. Sci. Instrum.* **1975**, *46*, 951.
(38) The slit image was set parallel to the lamellar interfaces and the scattering profiles were taken along the direction normal to the interfaces. Under this condition, the slit-smearing effect is minimum and almost negligible because of a very high degree of lamellar orientation.
(39) Hosemann, R.; Baguchi, S. N. "Direct Analysis of Diffraction by Matter"; North-Holland Publishing Co.: Amsterdam, 1962.
(40) Cotton, J. P.; Decker, D.; Benoit, H.; Farnoux, B.; Higgins, J.; Jannink, G.; Ober, R.; Picot, C.; des Cloizeaux, J. *Macromolecules* **1974**, *7*, 863.
(41) Guinier, A.; Fournet, G. "Small-Angle Scattering of X-rays"; Wiley: New York, 1955.
(42) Ballard, D. G. H.; Wignall, G. D.; Schelten, J. *Eur. Polym. J.* **1973**, *9*, 965.
(43) In order to circumvent this difficulty, it is highly desirable to deuterate polyisoprene or polybutadiene block chain. This deuteration gives the possibility of matching the contrast between the polystyrene microdomain and the polyisoprene or polybutadiene microdomain by mixing the deuterated and nondeuterated block polymers in an appropriate proportion.
(44) Debye, P. *J. Phys. Colloid Chem.* **1947**, *51*, 18.
(45) See, for example: de Gennes, P.-G. "Scaling Concepts in Polymer Physics"; Cornell University Press: Ithaca, NY, 1979; p 37.
(46) Farnoux, B.; Boue, F.; Cotton, J. P.; Daoud, M.; Jannink, G.; Nierlich, M.; de Gennes, P.-G. *J. Phys. (Paris)* **1978**, *39*, 77.
(47) Richards, R. W.; Thomason, J. L. *Polymer* **1981**, *22*, 581.
(48) Bates, F. S.; Berney, C. V.; Cohen, R. E.; Wignall, G. D. *Polymer* **1983**, *24*, 519.
(49) The effects of deuteration on the single-chain measurements have recently been shown to be very significant in several systems (e.g., segregation effects of the labeled chain during crystallization,[50] a change of the cloud-point curve by deuteration of one of the components in polymer blends,[51] and so on). Such deuteration effects should not be significant in the system studied in this paper. The deuteration may slightly shift order–disorder transition points[11,13-15] of block polymer solutions possessing UCST-type behavior. However, such a slight change of the transition temperature or concentration would hardly cause segregation between deuterated block polymers and protonated block polymers under the solvent-casting conditions employed in this study. This speculation is supported from experimental evidences that two types of block polymers (e.g., α and β) having a fairly large molecular weight difference and therefore having a substantial difference in the order–disorder transition points can be molecularly mixed to form a microdomain of a single identity period and morphology under

the solvent-casting conditions or other film preparation conditions.[26,52,53]

(50) Shelten, J.; Wignall, G. D.; Ballard, D. G. H.; Longman, G. W. *Polymer* **1977**, *18*, 1111. Wignall, G. D.; Child, H. R.; Samuels, R. J. *Ibid.* **1982**, *23*, 957.

(51) Yang, H.; Hadziioannou, G.; Stein, R. S. *J. Polym. Sci., Polym. Phys. Ed.* **1983**, *21*, 159.

(52) Hasegawa, H.; Yamasaki, K.; Hashimoto, T., to be submitted to *Macromolecules*. Yamasaki, K.; Hasegawa, H.; Hashimoto, T. *Polym. Prepr. Jpn.* **1983**, *32*, 1691.

(53) Hashimoto, T. *Macromolecules* **1982**, *15*, 1548.

(54) In Figure 13, the data in wide q region were purposely shown. It should be noted that the horizontal scale is much more compressed than those used in Figures 11 and 12, resulting in an enhancement of the waviness of the data. If Figure 13 is plotted on the same scale as in Figures 11 and 12, the data fall on the straight lines. The criterion for Guinier's law (eq IV-3) for a homogeneous sphere was stated as $(qR_{gv})^2 \lesssim 1.3^2$ in the text. This criterion is fairly strict; within this criterion the error involved by Guinier's approximation should be less than 4.2% of the rigorous value. If one allows an error of about 15% in the intensity data on the logarithmic scale, the critical value will be much larger: $(qR_{gv})^2 \lesssim 5$; viz., R_{gz} should be obtained from $q^2 \lesssim 0.004$. Although we do not know the exact criterion for the anisotropic system under consideration, we adopted the criterion of $q^2 < 0.004$ to determine R_{gz}.

(55) **Note Added in Proof.** In connection with note 49 above, we have also found that the deuterated block polymer and the protonated block polymer, having different total molecular weights but nearly equal molar compositions, can mix molecularly in a single microdomain morphology. Hasegawa, H.; Hashimoto, T. *Kobunshi Ronbunshu* **1984**, *41*, 759.

Phase Separation in Low Molecular Weight Polymer Mixtures†

Thomas P. Russell* and Georges Hadziioannou

IBM Research Laboratory, San Jose, California 95193

William K. Warburton‡

Stanford Synchrotron Radiation Laboratory, Stanford, California 94304.
Received March 7, 1984

ABSTRACT: The initial stages of phase separation in low molecular weight mixtures of polystyrene (M_w = 2000) and polybutadiene (M_w = 1000 and 2500) have been examined by using time-resolved small-angle X-ray scattering. The high flux from a synchrotron source was utilized due to the rapid kinetics and the weak contrast at the early stages of phase separation. Over the scattering vector range studied (from q = 0.07 to 0.97 nm^{-1}) no evidence of a scattering maximum, characteristic of a periodic variation in the concentration, was observed. At the onset of phase separation, the intensity at a constant scattering vector was found to depend exponentially on time with an amplification factor $R(q)$ that changed from positive values at low q to negative values at high q. According to the Cahn-Hilliard theory,[1,2] these crossover points were used to estimate the spinodal temperatures and Flory-Huggins interaction parameters. Deviations of the scattering vector dependence of $R(q)$ strongly suggest that thermal density fluctuations not taken into account by the Cahn-Hilliard theory contribute significantly to the observed scattering.

Introduction

The kinetics of phase separation in polymer mixitures is not yet understood quantitatively. In contrast to the numerous theoretical and experimental treatments of this problem (see, for example: ref 3 and 4) for small molecular mixtures, the polymeric analogues have received relatively little attention. de Gennes[5] and, later, Pincus[6] have attempted to theoretically treat the kinetics of demixing in bulk polymer mixtures by modifying the existing Cahn-Hilliard theory.[1,2] Experimentally, Bank, Leffingwell, and Thies[7] first observed the reversible phase separation of high molecular weight polymer mixtures in the polystyrene (PS)/poly(vinyl methyl ether) (PVME) system using differential scanning calorimetry and dielectric relaxation. Subsequent to this, Nishi, Wang, and Kwei[8] using both optical microscopy and NMR[5] first examined the kinetics of phase separation in this mixture. From their studies, they concluded that the phase separation process could be adequately described in terms of the Cahn-Hilliard model. Gelles and Frank,[9] utilizing excimer fluorescence to probe the changes in local concentration as a function of time, confirmed these findings. Recently, Hashimoto and co-workers[10] extended studies on this mixture by small-angle light scattering (SALS) and quantitatively interpreted their results using the de Gennes-Pincus modification to the Cahn-Hilliard theory. On this same system, Snyder et al.[11,12] performed an extensive series of measurements using SALS. In contrast with previous work, they found that only the very early stages of phase separation could be described by the linearized theories. Incorporation of nonlinear terms was necessary in order to fully describe the process and, it may be argued, that the agreement between experiment and linearized theories was fortuitous.

While other polymer mixtures are known to possess lower critical solution temperatures (LCST) the LCST of PS/PVME conveniently occurs at temperatures well above the glass transition temperature and much lower than the decomposition temperature of either component. Consequently, there is little information available on the kinetics of phase separation for other high molecular weight polymer mixtures.

Phase separation in lower molecular weight polymer mixtures has been studied by Nojima and co-workers[13-16] using SALS. Mixtures of PS with poly(methylphenylsiloxane) (PMPS) were found to exhibit upper critical solution temperature (UCST) behavior. As expected, the rates of the phase separation were more rapid than with the higher molecular weight mixtures. However, they did not find agreement with the Cahn-Hilliard theory and required the nonlinear treatments[17-19] in order to quan-

† Some of the materials incorporated in this work were developed at SSRL with the financial support of the National Science Foundation (Contract DMR77-27489) (in cooperation with the Department of Energy).

‡ Present address: University of Southern California, Marina DelRey, CA 90292.

0024-9297/85/2218-0078$01.50/0